KCI CONCRETE JOURNAL
Vol.14 No.3, Sep. 2002, pp.111-120

Structural Behavior of Beam-Column Joints Consisting of Composite Structures

Seung-Jo Lee[1)], Jung-Min Park[1)], and Wha-Jung Kim[2)*]

[1)] *Dept. of Architectural Engineering, Kyungpook College, Korea*
[2)] *Dept. of Architectural Engineering, Kyungpook National University, Korea*

(Received January 18, 2001; Accepted August 7, 2002)

Abstract

This study proposes a joint model consisting of different types of members as a new structural system, and then investigates the resulting structural behavior. The joint model consists of a concrete-filled steel tube column (CFT) together with a steel reinforced concrete at the end plus reinforced concrete beam at the center. For comparison, two other joint models were designed, that are, a CFT with a reinforced concrete beam, and a CFT with a steel reinforced concrete at the end plus steel concrete beam at the center, then their joint capacity and rigidity, energy absorption capacity, etc., were all investigated. From the results, the CFT column with a steel reinforced concrete at the end plus steel concrete beam at the center was outstanding in terms of its capacity and rigidity. The results of this analysis demonstrate that an adequate connection type and reinforcement method with different materials of increasing the rigidity, thereby producing a capacity improvement along with protection from pre-fractures.

Keywords: joint rigidity, rotational resistance capacity of beam, moment-joint translation angle, collapse modes

1. Introduction

Recently, many high-rise, large-scale, and multifunctional urban buildings have been constructed in response to rapid economic growth and expansion. Thus, a large number of studies for new structural systems have been conducted using recently developed high-strength and high-performance materials. As a result, a composite structural system consisting of different types of member has received a lot of attention, because a composite structural system has certain superior structural properties as well as good productivity, execution efficiency, longer life span, and improved rigidity over existing structural systems.

However, a composite structure consisting of different structural members still has problems clearing the stress flow between its different members and in developing a beam-column joint model. Generally, in a composite structure, a CFT column is widely used with a reinforced concrete structure, while the beam is normally a H-steel shaped structure. While steel beams are effective when used in long-span structures, they have problems in producing good joint rigidity. In contrast, RC beams are more effective in developing joint rigidity; however, they have problems when used in long-span structures.

The test results in this study are important and useful to understand the structural behavior and capacity of beam-column joint in the three types of specimen. The study presents analytical and experimental a procedure to evaluate the structural behavior on the specimen of the beam-column joint and it was also evaluated the effect of parameters on this specimen.

Accordingly, it would appear that a mixture of steel and RC members would be ideal. However, at this point, there is no design method and system, which can combine complex stress mechanism and joint details. Therefore, to develop a new structural system, this study was proposed a joint model consisting of different types of members and investigated its structural behavior.

2. Program of experiments

2.1 Specimen plans

* *Corresponding author*
Tel.: +82-53-950-5596; Fax.: +82-53-950-6590
E-mail address: kimwj@kyungpook.ac.kr

In this study, a total of 27 specimens were planned with key parameters, including three types of connection beam member: RC (end) plus RC (center), SRC (end) plus RC (center), SRC (end) plus SC (center) and Breadth-thickness (B/t) ratio, and axial compression ratio (P/P_y=0.0, 0.3, 0.5), plus the strength of the concrete was fixed at 39.23N/mm^2, where SRC = steel reinforced concrete, SC = steel concrete. An outline of the test program is given in Table 1.

2.2 Connection type & detail

The connection was performed so that the welded main-reinforcement of the beam passed through the column. The steel tube column was a plate-welded joint. Therefore, the steel part was reinforced with high-capacity bolts on the reinforced plate welded in a steel web. The connection type and detail is shown in Fig. 1.

2.3 Test rig layouts and operation

The tests were performed in a reaction frame that comprised of two beam-end-linked actuators, as shown in Fig. 2. The strain measured position of each specimen was established by 2 LVDT transducers, 6 Wire Strain Gauges (W.S.G), on the left and right upper part of the column. Strain gauges were also used to predict the buckling and capacity of the specimens. In a case of a beam member of framework, 4 LVDT transducers were used to establish the left, right, upper, and lower ends of the beam for all the specimens. A W.S.G. displacement system was installed as a compressive reinforcement to measure the inner tension and plate face of the specimens, plus two more systems were set up on the concrete surface.

All tests were conducted under displacement control performed cyclic loading in steps of 1/100 radian every 1 cycle. The experiment was terminated after the automatic loading of 6 ~ 8cycles. The displacement control is shown in Fig. 3.

Table 1 Outline of test program

Specimen name	Size		Beam		H-Steel shaped (mm)	F_c (N/mm^2)	ACR (P/P_y)
	Beam (mm)	Column (mm)	End	Center			
A0RR1 ~ C5RR2	100 × 200	□-100×100×1.6 (B/t=62.5)	RC	RC	None	39.23	
		□-100×100×2.3 (B/t=43.5)					
		□-100×100×3.2 (B/t=33.3)					
A0SRR1 ~ C5SRR2		□-100×100×1.6 (B/t=62.5)	SRC	RC	H-150×75×5×7		0.0
		□-100×100×2.3 (B/t=43.5)					0.3
		□-100×100×3.2 (B/t=33.3)					0.5
A0SRS1 ~ C5SRS2		□-100×100×1.6 (B/t=62.5)	SRC	SC			
		□-100×100×2.3 (B/t=43.5)					
		□-100×100×3.2 (B/t=33.3)					

Note: A0RR1-A=(B/t=62.5); B=(B/t=43.5); C=(B/t=33.3); 0=ACR; RR=RC(end) plus RC(center); SRR=SRC(end) plus RC (center) SRS=SR(end) plus S(center); 1=Left beam; 2=Right beam; □ =Square steel tube

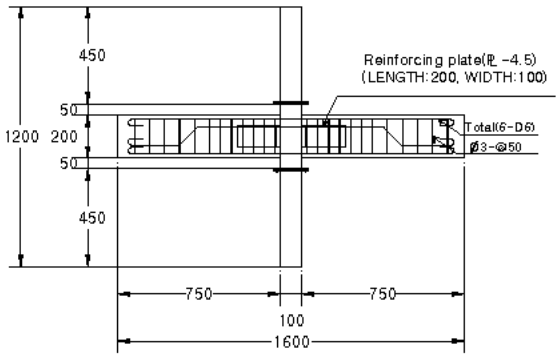

(RC plus RC specimen)

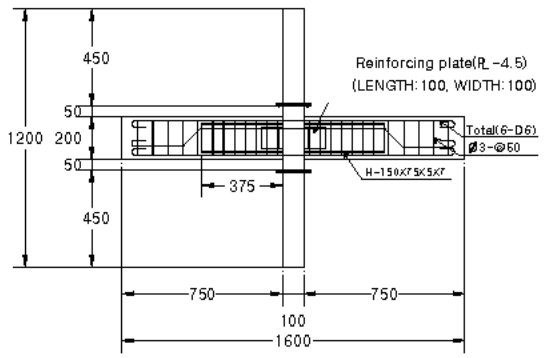

(SRC plus RC specimen)

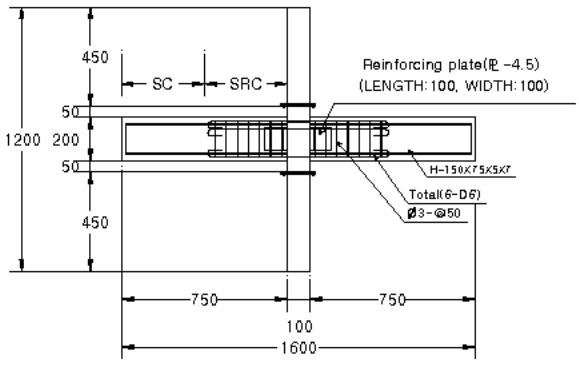

(SRC plus SC specimen)

Fig .1 Connection type and detail (Continued)

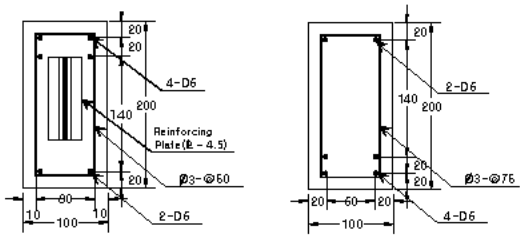

(Beam detail of RC plus RC specimen)

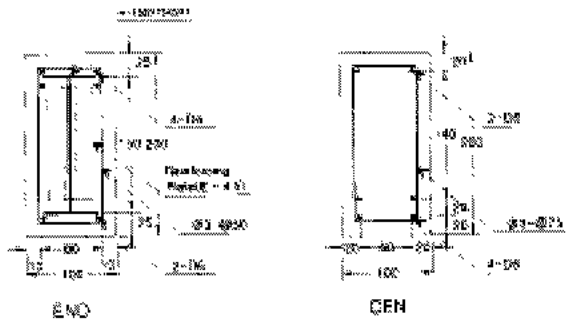

(Beam detail of SRC plus RC specimen)

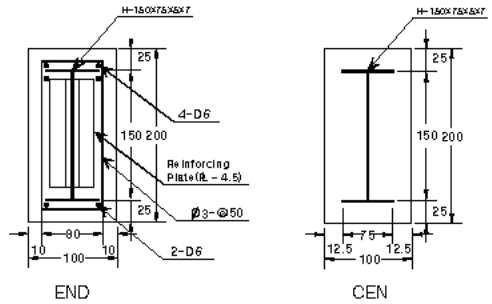

(Beam detail of SRC plus SC specimen)

Fig .1 Connection type and detail

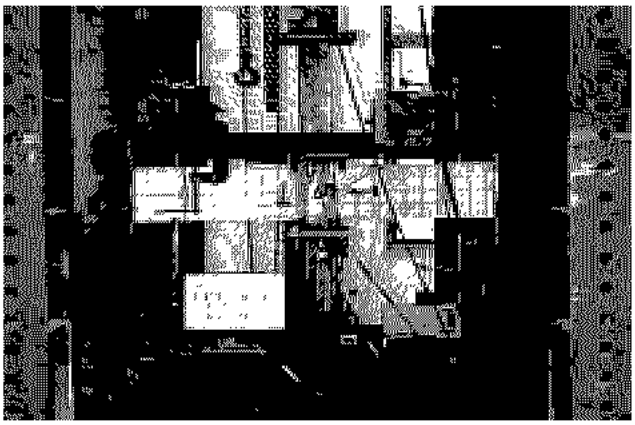

Fig .2 Schematic representation of test rig layout

2.4 Tension strength of steel tube

To determine the material properties, a tensile strength test was conducted on the steel tube, according to the standard *KS B 0801* (Korean Industrial Standards), from the upper and middle to the lower part for three cut-off

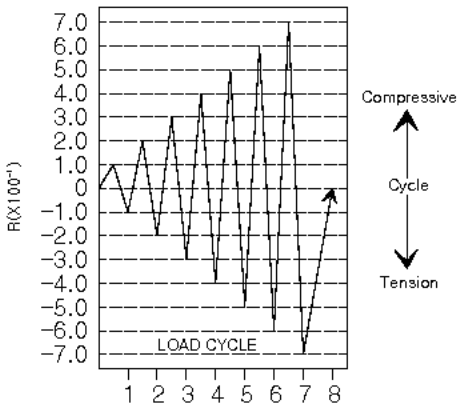

Fig .3 Displacement control

Table 2 Tensile strength of steel tube

Specimen		*(kN/mm²)	**(kN/mm²)	**/*	Elo (%)
Square steel tube	□ -100×100×1.6	0.40	0.51	1.265	18.6
	□ -100×100×2.3	0.37	0.47	1.267	22.1
	□ -100×100×3.2	0.36	0.44	1.195	21.4
H-shaped steel	Flange	0.45	0.52	1.152	21.6
	Web	0.36	0.405	1.124	22.4
Reinforcement plate	PL-4.5	0.41	0.413	1.019	18.2

Note) * =yielding strength; ** = tensile strength; Elo=elongation ratio

Table 3 Proportion and experimental results of concrete

Design strength (N/mm²)	MG (mm)	SP (mm)	Unit weight (kg/m³)						ST (N/mm²)	MS (%)
			C	Ag	S	G	W	A		
39.23	13	14	480	53	744	931	160	8	54.6	0.32

Note) MG=Maximum size of coarse aggregate; SP=Slump; C=Cement; Ag=Agent; S=Sand; G=Gravel; W=Water; A=High range water reducer; ST=Strain at ultimate strength; MS=Strain at the ultimate strength (%)

specimens. The results of the tensile strength test are shown in Table 2.

2.5 Compressive strength test of concrete

An experiment for testing the compressive strength of the concrete specimen 100ø ×200 (mm) was performed based on *KS F 2404*, to obtain the strength of the concrete used for the CFT specimens. The mix proportions and test results are shown in Table 3.

3. Experimental results and comments

3.1 Joint rigidity

The synthetic curve of the load-displacement relationship for all specimens, obtained using the method described by Naoki *et al.* (1997) is shown in Fig. 4. Where Q_{max}= maxi-

mum capacity point, Q_y= yield point, δ = strain (mm).

The overall results of the rigidities are summarized in Table 4 and Fig. 5. In relation to the B/t (Breadth-thickness) ratio, the rigidity was degraded, due to an increasing axial compression ratio. Generally, the capacity and initial rigidity in axial compression ratio (P/P_y=0.0) exhibited a large value difference with various increments of steel tube thickness. The initial rigidity for axial compression ratio (P/P_y=0.3, 0.5) was similar to the value changes.

The initial and plasticity rigidity for the SRC plus SC specimen, with H-shaped steel beam reinforcing in the center, was slightly higher than the values for the RC plus RC, and SRC plus RC specimens. It was observed that the maximum value of the initial rigidity was about 35.9% whereas the minimum value was about 30.2%, which was greater than that of the RC plus RC specimen. These results are significant as they reflect the difference in the inner reinforcing of the connection. The axial compression ratio and B/t increment were considered in the column member, where a brittle fracture produced the shear-force and capacity comparable with the experimental results. After the initial rigidity, these results decreased to the value for plasticity rigidity.

The results of this analysis demonstrate that an adequate connection type and reinforcing method is capable of increasing the rigidity, thereby improving the capacity of difference materials to protect against a pre-fracture.

3.2 Hysteretic behavior of joint

The beam-column connection indicated that the results resembled the hysteretic behavior shapes of the RC plus RC and SRC plus RC specimens, as seen in Fig. 6. In the case

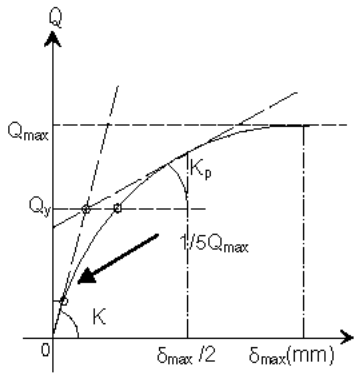

Fig .4 Rigidity and yield point

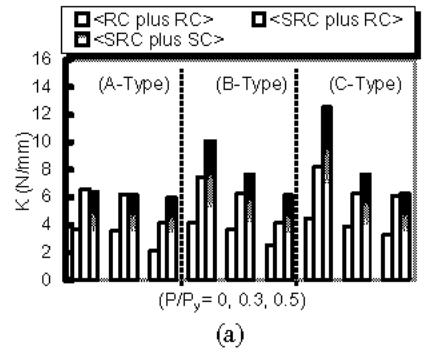

(a)

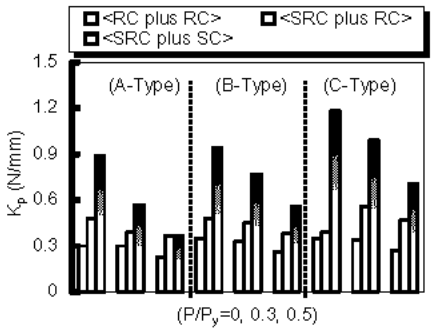

(b)

Fig .5 Axial compression ratio and rigidity

Table 4 Results of rigidity and experiment

Specimen name		K (N/mm)	K_p (N/mm)	Specimen name	K (N/mm)	K_p (N/mm)	Specimen name	K (N/mm)	K_p (N/mm)
B/t (62.5)	A0RR1	3.73	0.30	A0SRR1	6.59	0.48	A0SRS1	6.28	0.81
	A0RR2	3.53	0.30	A0SRR2	5.34	0.47	A0SRS2	6.37	0.89
	A3RR1	3.57	0.25	A3SRR1	5.33	0.38	A3SRS1	5.99	0.48
	A3RR2	3.48	0.30	A3SRR2	6.21	0.39	A3SRS2	6.23	0.57
	A5RR1	1.93	0.23	A5SRR1	3.92	0.37	A5SRS1	5.95	0.37
	A5RR2	2.11	0.21	A5SRR2	4.12	0.35	A5SRS2	5.98	0.36
B/t (43.5)	B0RR1	3.30	0.32	B0SRR1	5.95	0.41	B0SRS1	10.1	0.82
	B0RR2	4.14	0.35	B0SRR2	7.48	0.48	B0SRS2	9.80	0.94
	B3RR1	2.96	0.33	B3SRR1	6.28	0.45	B3SRS1	7.65	0.65
	B3RR2	3.69	0.28	B3SRR2	3.92	0.40	B3SRS2	6.72	0.77
	B5RR1	2.57	0.26	B5SRR1	4.16	0.38	B5SRS1	6.16	0.56
	B5RR2	2.26	0.24	B5SRR2	3.99	0.39	B5SRS2	6.00	0.43
B/t (33.3)	C0RR1	4.51	0.35	C0SRR1	7.76	0.56	C0SRS1	9.90	1.09
	C0RR2	3.75	0.32	C0SRR2	8.24	0.53	C0SRS2	12.55	1.18
	C3RR1	3.90	0.30	C3SRR1	4.05	0.47	C3SRS1	7.14	0.99
	C3RR2	3.16	0.34	C3SRR2	6.29	0.47	C3SRS2	7.69	0.93
	C5RR1	3.26	0.25	C5SRR1	6.11	0.39	C5SRS1	6.28	0.59
	C5RR2	3.21	0.27	C5SRR2	5.75	0.40	C5SRS2	6.15	0.71

Note: K_p=Plasticity rigidity; K=Initial rigidity

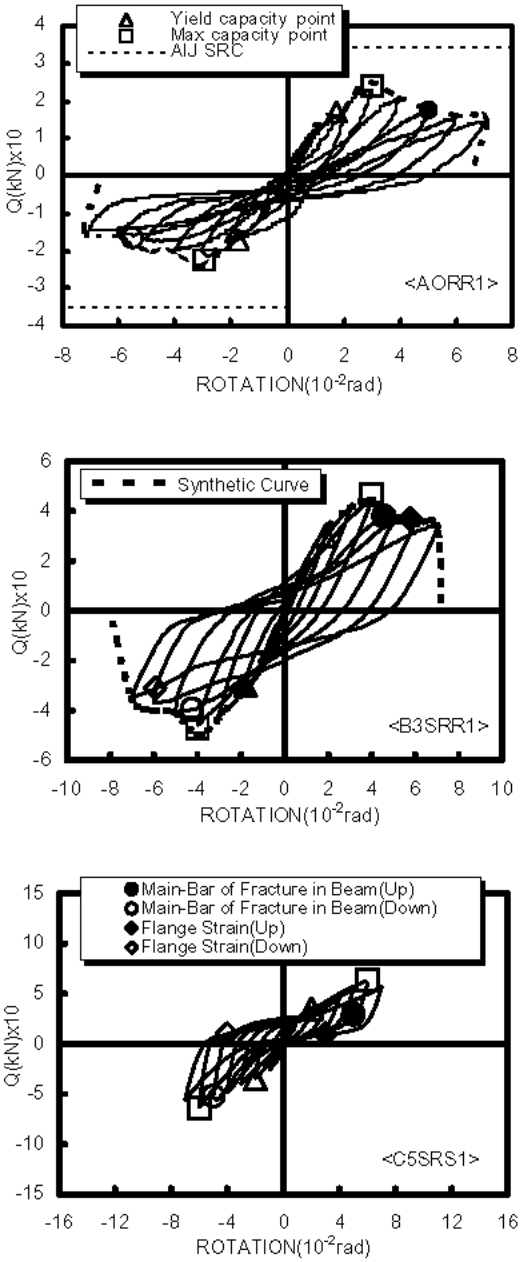

Fig .6 Shear capacity-joint translation angle

of the A-Type specimen, the hysteretic behavior generally showed a stable bi-linear curve, yet the axial compression ratio large specimen exhibited a tri-linear curve. For the B-Type and C-Type specimens, the shape of the hysteretic behavior was a stable spindle shaped curve for small axial compression ratios, the same as the previous results up to the maximum capacity point, however it became a tri-linear curve with an unstable S-shape above the maximum capacity, as with the strain for the main-reinforcement.

Under cyclic loading, the SRC plus RC members exhibited a bi-linear curve with a spindle shape, and remained stable with hysteretic behavior up to the maximum capacity point. Also, the A-Type specimen exhibited to no relation to the B/t and axial compression ratio with a steel tube and manifested unstable behavior in an S-shaped tri-linear curve, whereas the B- and C-Types, as previously mentioned, showed a similar tendency in the RC plus RC and SRC plus RC specimens. It was noted that this behavior was related to the type of reinforcing in the beam-column connection, as will be seen in a later section (SRC plus SC). Moreover, these facts are consistent with those observed in previous theses.[3)]

3.3 Rotation resistance capacity of beam

Fig. 7 shows the plot for the rotation of the beam member of framework, and the mutual values were compared at each initial crack point, yield point, and at 80% of the maximum capacity. As seen from the figure, the rotation angle of the member almost completely resembled the specimen at the initial crack-point, while in the case of yielding it gradually increased experiment 1 (beam member: RC plus RC) < experiment 2 (beam member: SRC plus RC) < experiment 3 (beam member: SRC plus SC) with the same B/t and axial compression ratio. The maximum capacity was similar to the yield point and showed values ranging between 30% and 100 %, compared with experiment 1.

Accordingly, it would appear that the use of adequate reinforcing was effective in improving the rotation angle of the beam member and the capacity performance of beam-column. In contrast, as can be seen from the plot, even though the joint translation limit-angle evaluation passed the 80% of the maximum capacity, 5/100 radian values were observed in the plot in experiment 1 and experiment 2, whereas experiment 3 increased from 20% to 40% when it was compared with experiment 1.

Accordingly, the H-steel shaped reinforcing beam exhibited a higher joint rotation resistance capacity as the strain increased, comparing with the non-reinforcing of the RC beam.

3.4 Collapse modes

3.4.1 Beam (RC plus RC and SRC plus RC)-column

It is known that the failure characteristics of a joint are useful in understanding the hysteretic behavior. Collapse modes occurred with a 2-cycle hysteretic behavior, that is, a minute crack on the surface specimen, which reached a maximum capacity point after 3rd cycle, also the strain of main reinforcement presented in the plot between cycles 4 and 5, showed that the specimen collapsed together with a main reinforcement fracture in a 5-cycle curve. All specimens exhibited a surrounding connection with the transverse tension crack and shear present in the beam center

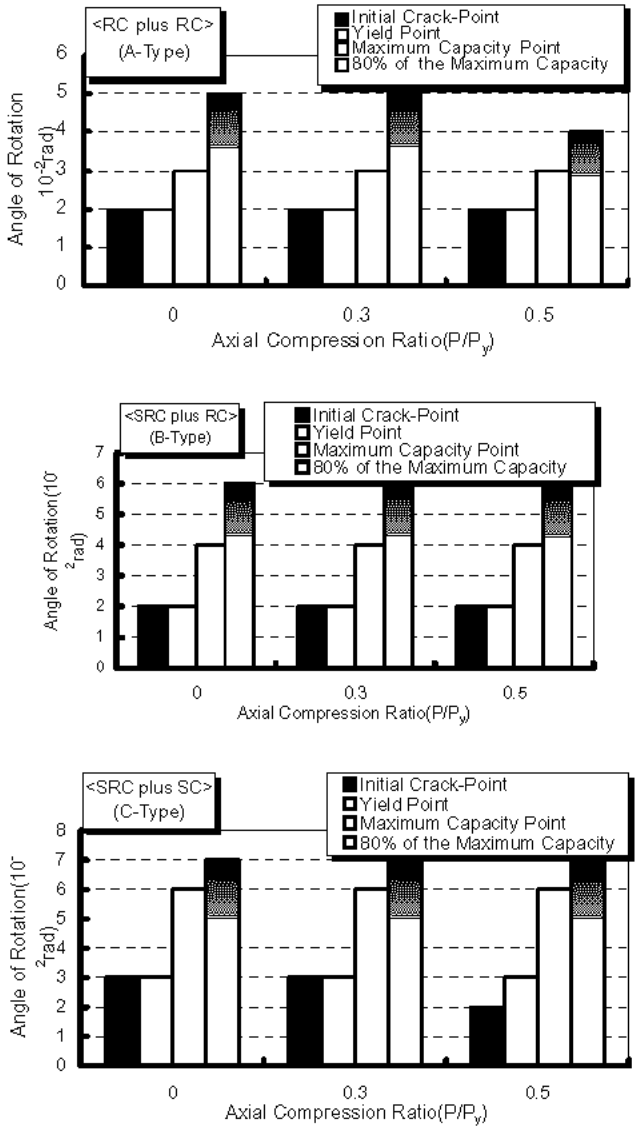

Fig .7 Rotation resistance capacity of beam

after the transverse tension crack was shaped. With the SRC plus RC specimens, in the case of a small axial compression ratio (P/P_y=0.0), the collapse modes occurred prior to the shear crack in the surrounding connection that presented a transverse tension crack and diagonal on the beam center, whereas a high-axial compression ratio showed the opposite tendency.

3.4.2 Beam (SRC plus SC)-column

Most of the hysteretic behavior in the specimens occurred after 2 cycles with a bending-crack on the surface concrete surrounding the upper and lower parts, and between the H-steel-shaped flange area and concrete boundary in a 3～4-cycle curve with a mixed horizontal and diagonal crack(20~40°). A 5～6-cycle hysteretic curve produced the maximum capacity point of the main reinforcement fracture and H-steel shaped strain, which was

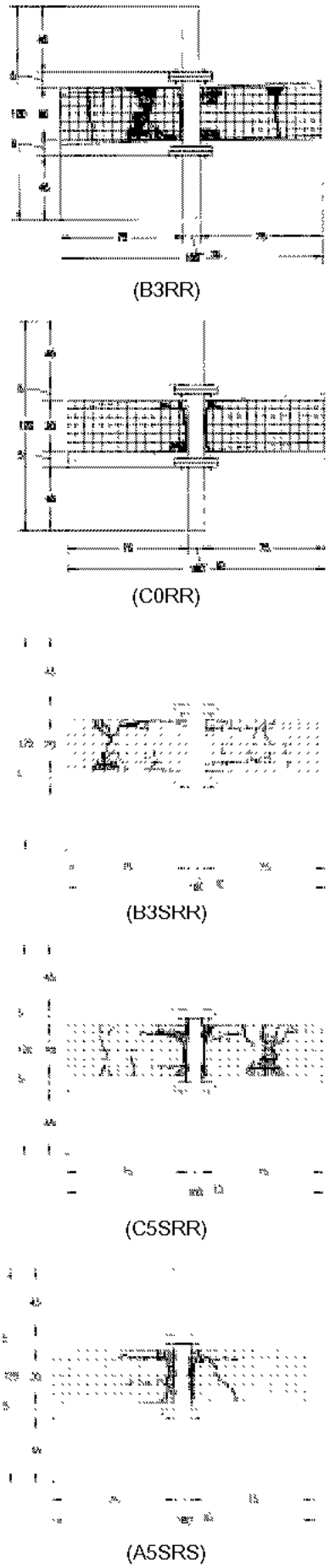

Fig .8 Collapse modes(continued)

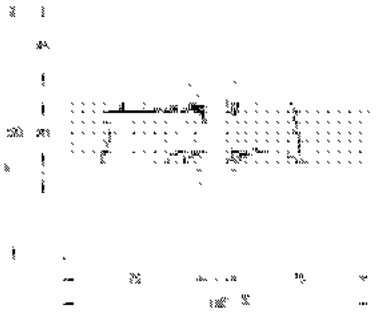

(C3SRS)

Fig .8 Collapse modes

completely presented by a separation of the flange area welding portion in the connection area, before and after the maximum capacity point.

3.5 Moment-joint translation angle

The experimental values of the beam-column joint obtained from the various specimens with the cyclic loading of the beam are summarized in Fig. 9. In the case of axial compression ratio (P/P_y=0.0), the plastic moment "${}_bM_p$" and seismic performance evaluation method, i.e., ACI(R=0.035), NEHRP Recommended Provisions(R=0.02), National Building Code of Canada(R=0.02), and Japanese Building Standard Law(R=0.005) were examined respectively according to the structural law experiment in the moment-resisting frame to establish the maximum displacement angle of the member (R). The "${}_bM_p$" and "R" investigated in these paragraphs are assumed to be the bending moment, and their section area in the elastic stress can be expressed as follows:

$$ {}_bM_p = Z_p \cdot \sigma_y \tag{1}$$

$$ Z_p = \frac{B^2 d}{4} \tag{2}$$

$$ Z_p = \{B_f t_f (d - t_f)\} + \left\{\frac{(d - 2t_f)^2 t_w}{4}\right\} + \{0.4292 r^2 (d - 2t_f - 0.4467 r)\} \tag{3}$$

where Z_p and t_f are the plastic section coefficient in various sections and thickness of the flange, respectively, t_w is the web thickness and σ_y is the yielding stress in the experimental result, B is one width of the rectangle section of the H-shaped steel section, d is the section height, and r is the fillet length. The plastic moment versus the joint rotation angle of the beam hysteretic curves for the three test specimens is shown in Fig. 9. From plot (c), it can be

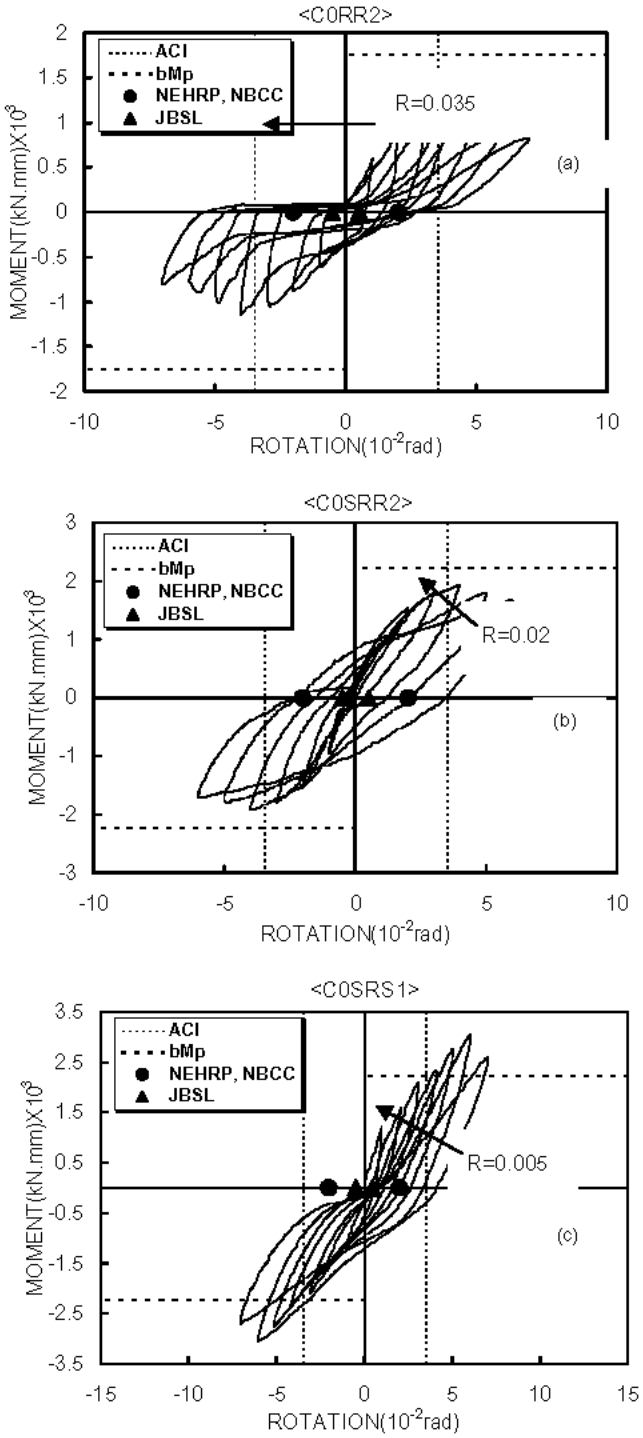

Fig .9 Moment-joint rotation angle

observed that the effect of the H-steel shape and reinforcing plate is significant. Moreover, a comparison of plot (a) to (b) with plot (c) indicates that the SRC plus SC specimens exhibited a more stable behavior and higher moment value than the RC plus RC and SRC plus RC specimens. According to the seismic performance law, the joint rotation angle value of a beam must pass the permitted legal value in both the left and right beam specimens. Therefore, from the perspective of rigidity and capacity, the SRC plus SC connection demonstrated a comparatively stable joint behavior.

4. Evaluation of joint capacity

This paper also evaluated the capacity of the beam-column joints through adequate reinforcing for the inner beam and panel zone. For each specimen, a capacity analysis was performed using the 9 respective experimental values in Table 5 to obtain expressions in terms of the bending capacity and shear superimposed capacity, by applying the Architecture Institute of Japan (AIJ) standard value [7] of a beam-column joint. The resulting high capacity values of the left and right beams are presented in Table 5.

4.1 Beam (RC plus RC)-CFT column connection

The inner beam RC is assumed to be responsible for the bending moment, and the joint panel-zone charge partially responsible for the shear capacity of the region of the steel web is due to the welding. These assumptions account for the remaining force for the joint shear capacity relative to the design method that produces a bending fracture model that has a safe value for a joint capacity evaluation in the RC part. In this capacity evaluation of the beam inner RC part, the values showed a bending capacity of about 15~19% in comparison with superimposition evaluation, this value was underestimated in order to gain a safe value, however, there is a slight tendency to overestimate when using the AIJ law.

4.2 Beam (SRC plus RC)-CFT column connection

The joint problem predicted by the shear fracture, when the steel lost its shear capacity in the SRC design method, showed the steel web as responsible for the occurrence of the steel shear capacity for the moment and the RC part as responsible for the shear capacity in the inner RC. However, the steel shear over estimated the shear stress transmitted by a large stud analysis for a RC beam. Plus, different types of structure were improved through the adequate shear reinforcing and harmonious capacity flow provided by a point shaped beam-column joint plastic hinge in the panel zone part.

On the basis of these concepts, the ultimate shear capacity evaluation investigated a capacity evaluation of the elements, the AIJ SRC law equation, and the experimental values. The evaluation based on the connection capacity was checked with the results listed in Table 5; from it can be observed that the safe value results had a tendency to be underestimated in the SRC law evaluation. The bending capacity for the RC part of the inner beam and the superimposed steel part superimposed showed an experimental capacity range of 52~57%. Therefore, when considering the shear, the capacity evaluation of the different types of member depended on superimposing the bending capacity (RC plus S) for each composition element. Plus, in the case of the existence of axial compression ratio, stable values were obtained for the specimens with the introduction of a reduction-coefficient for the superimposed theoretical value. In the AIJ 1987 law, a capacity equation of connection is recommended as the standard for the structural calculation of SRC structures. This capacity equation of a joint is defined as follows:

$$ {}_{c}V_{e}(2f_{t}\times{}_{t}\delta+{}_{w}P\cdot{}_{w}f_{t})+{}_{t}V\cdot{}_{s}f_{t} \quad (4) $$

$$ {}_{c}V_{e}=\left\{\frac{({}_{c}b+{}_{B}b)}{2}\right\}\times{}_{mB}d\cdot{}_{mc}d \quad (5) $$

$$ {}_{t}V={}_{t}t_{w}\cdot{}_{s}d\cdot{}_{s}d \quad (6) $$

4.3 Beam (SRC plus SC)-CFT column connection

As can be seen from Table 5, three different types of test exhibited remarkable capacity improvement, i.e., A0SRS, B0SRS, and C0SRS. This study promoted rigidity and capacity to stiffen RC for steel structure end to increase rigidity of long spanned steel beam, and welted to steel flange to anchor U-shaped main reinforcement of structure end to easy stress flow between the different type structures. The joint model showed an experimental capacity of 33.2~

Table 5 Evaluation of joint capacity

Specimen name	RC (kN)		S (kN)		Joint capacity (kN)			Calculated/ measured
	$_{R}M_{0}$	$_{R}Q_{A}$	$_{S}M_{0}$	$_{S}Q_{A}$	(a)	(b)	(c)	
A0RR	4.23	12.45	None	None	33.83	4.23	22.39	0.189
B0RR					33.67		24.59	0.172
C0RR					33.48		28.12	0.150
A0SRR	3.95	49.42	20.91	92.37	34.12	24.86	43.75	0.568
B0SRR					33.93		46.79	0.531
C0SRR					33.78		47.59	0.522
A0SRS	3.95	49.42	20.91	98.96	18.56	24.86	54.52	0.456
B0SRS					18.53		65.14	0.384
C0SRS					18.49		74.95	0.332

Note: RC=reinforced concrete, S=steel, $_{R}M_{0}$=moment of RC part, $_{R}Q_{A}$=shear of RC, $_{S}M_{0}$=moment of steel part, $_{S}Q_{A}$=shear of steel, (a)=AIJ law, (b)=superimposed capacity, (c)=experimental capacity.

45.6% as an increment B/t ratio in the case of the bending capacity evaluation for both the RC part and the superimposed steel part. This demonstrates the importance of including the effects of the connection reinforcing type in an analysis to obtain a proper joint capacity evaluation method through B/t, axial compression ratio.

$$\left\{\frac{({}_{c}b\times {}_{sB}d\times {}_{mc}d)}{2}\right\}(2f_{s}\cdot {}_{J}\delta+{}_{w}P\cdot {}_{w}f_{t})+{}_{J}t_{w}\cdot {}_{sB}d\cdot {}_{sc}d\times {}_{s}f_{s} \qquad (7)$$

5. Conclusions

Based on the test results the following conclusions were made:

1) The results of this analysis demonstrate that an adequate connection type and reinforcing method with different materials are capable of increasing the rigidity, thereby producing a capacity improvement along with protection from pre-fractures.
2) Accordingly, the use of adequate reinforcing is effective in reducing the rotation angle of a beam member and the capacity performance etc. of the beam-column joint.
3) As shown in the plot, even though the joint rotation limit angle evaluation passes the 80% of the maximum capacity, a 5/100 radian value was observed in the plot in experiment 1 (RC plus RC), and experiments 2 (SRC plus RC) and 3 (SRC plus SC) increased respectively from 20% to 40% in contrast to experiment 1.
4) In the case of a small axial compression ratio (P/P_y=0.0) the collapse modes occurred prior to the shear crack in the surrounding connection that presented transverse tension and diagonal cracks on the beam center, however, the high-axial compression ratio showed the opposite tendency in the SRC plus RC specimens. In contrast, SRC plus SC specimen a hysteretic curve, in the 5~6cycles, produced the maximum capacity point with the main-reinforcement fracture and strain of H-steel shape, which was presented completely by the burst flange-welding portion with maximum capacity in the connection area.
5) Beam specimen displacements are reduced, considerably, from local buckling of column and deformations as increment of axial compression ratio, which do not contribute to increase an energy absorption capacity. According to seismic performance law, the joint rotation angle values pass that permit law value in left beam specimen and right.
6) An equation was investigated to understand the capacity of the internal beam-column joint. The resulting equation for calculating the capacity in the three types of specimen produced a satisfactory correlation between the calculated values and test results.

Acknowledgements

The authors would like to express their gratitude to the construction section of SAMSUNG Productions for providing the necessary economic resources needed to conduct the present study.

Notation

${}_{B}b$ = width of beam, mm
${}_{c}b$ = width of column, mm
${}_{mB}d$ = distance of beam up and down for main reinforcement, mm
${}_{mc}d$ = distance of column right and left for main reinforcement, mm
${}_{sB}d$ = beam flange of center distance, mm
${}_{sc}d$ = column flange of center distance, mm
$2f_s$ = allowable shear stress of concrete, kN/mm^2
${}_{s}f_s$ = allowable shear stress of steel, kN/mm^2
${}_{w}f_t$ = allowable tension stress of shear reinforcing in reinforcing-bar, main reinforcement, kN/mm^2
${}_{J}\delta$= beam-column joint a coefficient of shape
${}_{w}P$ = ratio of reinforcing-bar
${}_{J}t_w$ = beam-column joint web thickness of steel, mm
${}_{c}V_e$ = beam-column joint efficiency volume of concrete
${}_{s}V$ = web volume of beam-column joint steel, mm^3

References

1. Michel Bruneau., Chia-Ming Uang ., and Andrew Whittaker., "*Dutch Design of Steel Structures*," McGraw-Hill, 1998.
2. Naoki, TANAKA., Seiji, AKIYAMA., and Yasumi, SHIMURA.,"Structural Property of H-Shaped Beam to Box Column Connections with High-Strength Blind Bolts," *Journal of Structural and Construction Engineering,* Architectural Institute of Japan, 1997, pp. 121-128 (In Japanese).
3. Lee, S. J., Park, J. M., and Kim, W. J., "The Study on Behavior Properties of Joint Consisting of the Concrete Filled Steel Tube Column and R.C Beam,"*Journal of Korean Society of Steel Construction,* Korean Society of Steel Construction, 1997, pp. 177-186.
4. *NEHRP Commentary on the Guidelines for the Seismic Rehabilitation of Buildings,* Applied Technology Council, San Francisco, California, 1996.
5. *NEHRP Recommended Provisions for the Development of Seismic Regulations for New Buildings,* Federal Emergency Man Agency, Building Seismic Safety Council, Washington, D.C, 1994.
6. AIJ, *Recommendations for Plasticity Design of Steel Structures,* Architectural Institute of Japan, 1996(In Japanese).
7. AIJ, *Standard for structural calculation of steel reinforced concrete structures,* Architectural Institute of Japan, 1987.
8. Chia-Ming Uang., "Establishing R(or RW) and cd Factors

for Building Seismic Provisions," *Journal of Structural Engineering*, ASCE, 1991, pp. 19-28.
9. Attard, M.M. and Setunge, S., "Stress-strain relationship of confined and unconfined concrete," *ACI Material Journal*, V. 93, No. 5, 1996, pp. 432-442.
10. *Guidelines to Structural Calculation under the Building Standard Law,* Building Center, Tokyo, Japan, 1994.
11. Chen, W.F., and Atsuta, F., "*Theory of beam-Columns,*" Vol. 1: In-plane behavior and design. McGraw-Hill, New York, 1976.
12. Charles W. Roeder, Brad Cameron, and Colin B. Brown., "Composite action in concrete filled tubes," *Journal of Structural Engineering., ASCE,* V.125, No. 5, 1999, pp. 477-484.
13. Brian Uy., "Strength of concrete filled steel box columns incorporation local buckling," *Journal of Structural Engineering., ASCE,* V.126, No. 3, 2000, pp. 341-352.
14. ACI Committee 318, *Building Code Requirements for Reinforced Concrete*, ACI 318-95, American Concrete Institute, 1995.